

Autonomous Millimeter Scale High Throughput Battery Research System

Fuzhan Rahmanian^{1,2,4,5,6*}, Stefan Fuchs^{1,2}, Bojing Zhang^{1,2,4,5,6}, Maximilian Fichtner^{1,3}, and Helge Sören Stein^{4,5,6*}

¹Helmholtz Institute Ulm, Applied Electrochemistry, Helmholtzstr. 11, 89081 Ulm, Germany

²Karlsruhe Institute of Technology, Institute of Physical Chemistry, Fritz-Haber-Weg 2, 76131 Karlsruhe, Germany

³Karlsruhe Institute of Technology, Institute of Nanotechnology, , 76021 Karlsruhe, Germany

⁴Technische Universität München, School of Natural Sciences, Department of Chemistry Lichtenbergstr 4, 85748 Garching, Germany

⁵Technische Universität München, Munich Data Science Institute, Walther-von-Dyck-Straße 10, 4, 85748 Garching, Germany

⁶Technische Universität München, Munich Institute for Robotic and Machine Intelligence, Georg-Brauchle-Ring 60-62, 80992 Munich, Germany

* corresponding author(s): Helge Sören Stein (helge.stein@tum.de), Fuzhan Rahmanian (fuzhan.rahmanian@tum.de)

Supplementary Information

1 Technology Stack

The autonomous millimeter scale high-throughput battery research system (Auto-MISCHBARES) project, accessible over GitHub at <https://github.com/fuzhanrahmanian/MISCHBARES>, is a Python-based web application developed on top of hierarchical autonomous laboratory automation and orchestration (HELAO)¹, which uses FastAPI² and leverages asynchronous Uvicorn³ as Asynchronous Server Gateway Interface (ASGI) for handling the flow of electrochemical experimentation. The logical representation of Auto-MISCHBARES is divided into Hubs, each dedicated to a specific task yet sharing a common codebase. Central is the ServerHub, which utilizes FastAPI² for task delegation and hosts user interfaces for experimental definition developed with Flask⁴, Node.js, HTML, and CSS for web-based interactions. It also encompasses a live visualizer build with bokeh⁵ package leveraging WebSockets⁶. The DeviceHub manages connectors for the different devices and acts as an intermediary between the equipment and the ServerHub. It enables Ethernet connections to the Hamilton Pump system <https://www.hamiltoncompany.com/laboratory-products/microlab-600/syringe-pump> and COM serial port connections to the stepper motor <https://www.owis.eu/en/>. Both systems are controlled using the API and DLLs provided by the manufacturer. The Metrohm potentiostat https://www.metrohm.com/de_de/products/a/ut30/aut302n_s.html is controlled by the Autolab SDK and the Metrohm DLLs. All DLLs are imported using pythonnet⁷, allowing C# compiled code to be integrated. The DataHub utilizes NumPy⁸ and Pandas⁹ for data processing and connects to a local PostgreSQL database¹⁰ via the psycopg2¹¹ database adapter. The MultiAnalyticHub utilizes a range of open-source packages, including OpenCV¹² for motion detection and Modular and Autonomous Data Analysis Platform (MADAP)¹³ for electrochemical analysis, enhanced by scikit-learn¹⁴ and SciPy¹⁵ for statistical parameter computation. Extensive unit and functional testing is implemented with the pytest package¹⁶. Documentation is available at <https://fuzhanrahmanian.github.io/MISCHBARES/>.

2 Operational guidelines

Researchers interested in the usage of Auto-MISCHBARES must first configure the `main_config.py` file with the correct IP addresses for the devices, paths to the manufacturers' DLLs, detailed quality control settings if desired, provide admin user credentials, password, and address for a hosted PostgreSQL database¹⁰, and give the Telegram API and Chat ID as environmental variables. Python packages listed in the `requirements.txt` file should be installed within the desired environment, and the Web user interface (UI) (Fig. 1) can be started by executing the `app.py` file. This UI consists of a login portal and a configuration panel. The login section secures user access, requires credentials for system entry, and ensures experiment accountability. Users can define general settings in the main configuration panel, generate measurement grids, and manage experimental parameters across multiple batches. The settings allow for the specification of individual experiments and their parameters within each batch. Users can run the experiment, save and retrieve configurations which are written as JSON formatted files picked up by the Auto-MISCHBARES application once the experiment begins. The `main.py` file serves as the entry point for running experiments, controlling the start and shutdown of all involved actions and servers, and performing the configured sequence of experiments. After the initial movement of the Scanning Droplet Cell (SDC) head, quality control for material sufficiency will display the camera feed for movement detection. Following wiping, the live visualizer will asynchronously display the voltage until contact is established. Subsequently, the visualizer will also display the live measurement. If quality checks fail, the orchestrator will either suspend the experimentation or stop it completely, depending on the scenario. After each measurement, analysis is performed on the fly, and results and raw data are stored in their respective tables in the database. All records are decorated with a Unique Identifier (UID), and each experiment acts as the primary key for its performed measurements, which in turn serves as the primary key for the collected analysis and raw data. Reports of the analysis will be plotted and saved in the configured folders, and the logged-in researcher will be notified of the progress. This process will be repeated until all the defined sequences of the experiment are performed. Upon completion, servers are shut down automatically, and an additional `.hdf5` file will be logged with all the experimental run's input, output, and metadata. A live demonstrative run, including a detailed tutorial, can be found on YouTube at https://www.youtube.com/watch?v=dMZ1WIy7i5s&ab_channel=FuzhanR.

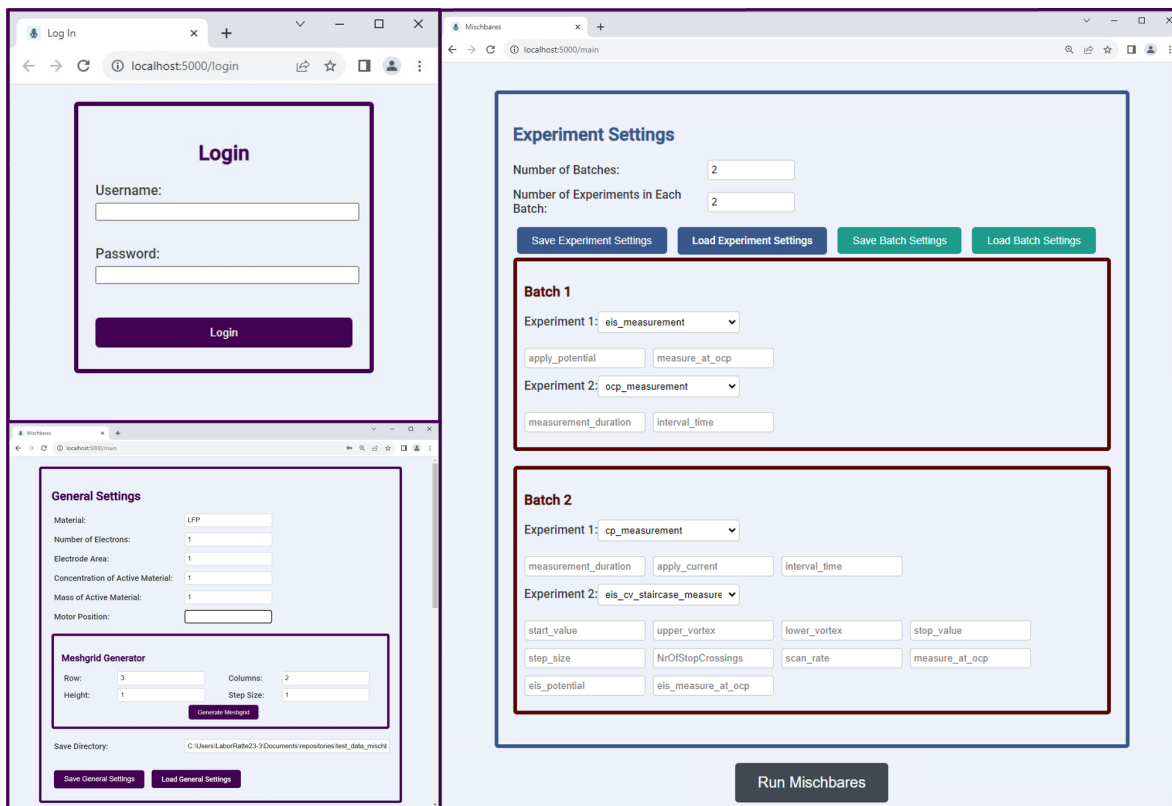


Figure 1: User Interface of the Auto-MISCHBARES system

3 XRF test measurement

X-ray Fluorescence (XRF) mapping was performed using a HORIBA XGF-900 micro X-ray Fluorescence Analytical Microscope (μ -XRF, Horiba Scientific, Japan). The spectra were acquired using a Rh source with an energy of 50 kV and 100 μ m polycapillary optics without an energy filter. The XRF elemental maps depicted in Supp. 2 show the distributions of Fe, Cr, Mn, Ni, Al and P on the screen-printed LFP electrodes. Fe and P show their highest intensities as circular points of 1.5 mm diameter in a 11x11 grid with a spacing of 4.9 mm correlating to the screen-printed LFP electrodes. Here, P is exclusively observed on these spots, while Fe can also be observed at a low intensity on the space surrounding that area. Cr, Mn, Ni, Al can be observed on the space surrounding the circular points. This area corresponds to the exposed Al-foil and Cr, Mn, Ni and the Fe observed, are related to impurities from the machining process of the foil as these are common components of stainless steel.

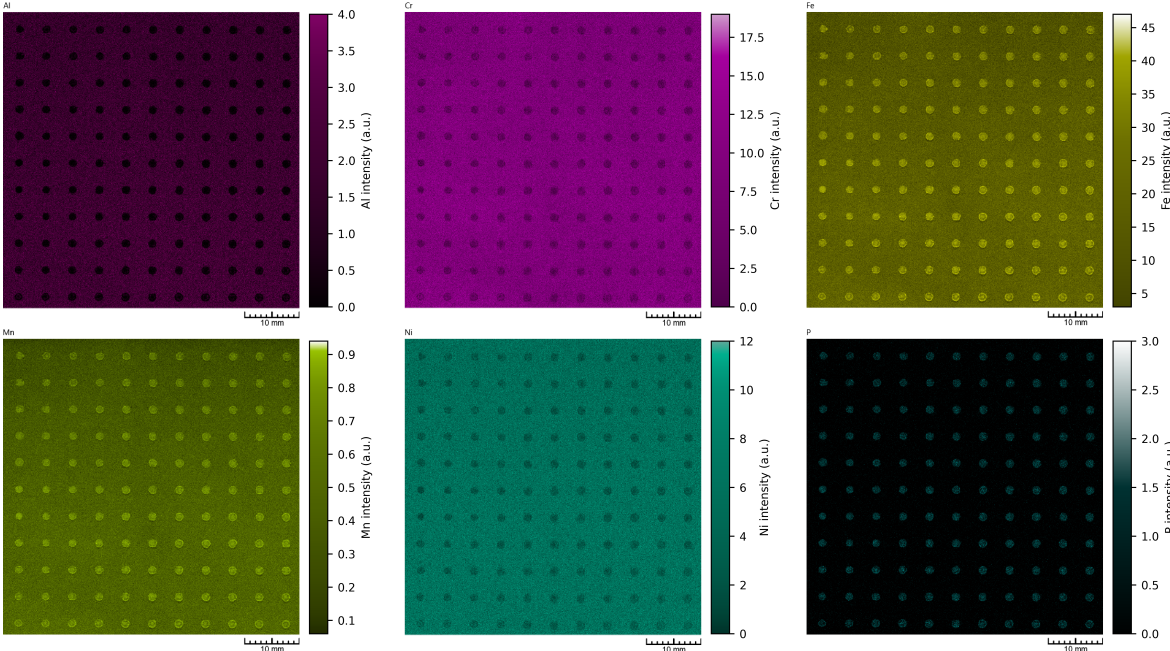


Figure 2: XRF elemental distribution maps of the screen-printed LFP electrodes showing the distribution of Al, Cr, Fe, Mn, Ni, and P. Bright colors show high concentrations, while dark colors show lower concentrations. The coated points can be observed as circular spots in the elemental maps, where the presence of overlying active material reduces the background to negligible levels. Notably, the spatial distribution of Mn and Fe possess comparable patterns, which can be explained due to their comparable ionic radii and chemical affinities. Despite this similarity, the signal intensity of Mn is significantly lower compared to Fe, which indicates different concentration levels within the sample. Subtle differences in their spatial distribution may relate to the manufacturing process.

4 Electrode production

The screen printing mask was prepared by applying the mask emulsion (FLX Screen hybrid-fotoemulsion) onto a 43T/110 silk net mesh, subsequently drying it in a dark room, and then hardening it through exposure to ultraviolet (UV) light. Circular holes were imprinted onto the mask to serve as electrodes.

4.1 Preparation of the LFP electrodes

For the fabrication of the cathode working electrode, a homogeneous slurry was prepared. This slurry comprised LFP, Carbon Black, and Carboxymethylcellulose (CMC, Sigma-Aldrich, medium viscosity) as a binder, in a weight ratio of 8.5 : 1 : 0.5, respectively. Milli-Q water (18.2 M Ω cm) was utilized as the solvent. The mixture was subjected to a two-cycle blending process in a Planetary Centrifugal Mixer (Thinky, ARE250), with each cycle consisting of a mixing phase at 1500 rpm for 10 minutes and a defoaming phase at 400 rpm for 1 minute. Subsequently, the Aluminum foil, employed as the current collector, was etched in a 1 M KOH solution for a minute to enhance surface roughness, thereby

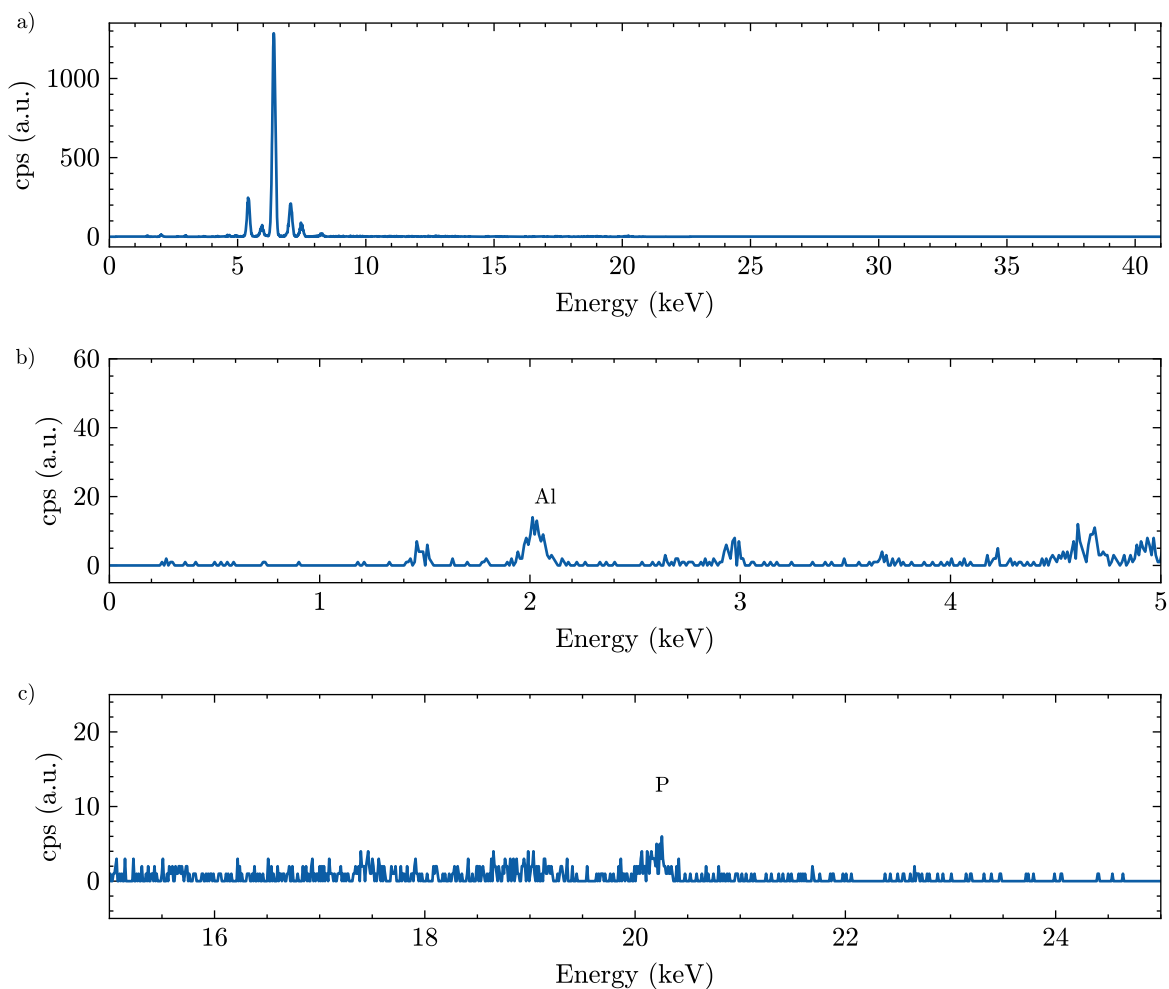


Figure 3: Averaged XRF spectrum representing cumulative signals from one of the screen-printed spots, highlighting characteristic X-ray peaks. a) Showing the whole spectral region, b) inset highlighting the minor contribution of Al and c) P signals.

augmenting adhesion and reducing slurry dispersion. Post-etching, the foil was thoroughly rinsed with distilled water to eliminate residual hydroxides. The prepared slurry was then uniformly screen-printed onto the Aluminum foil. The electrodes were subsequently dried at atmospheric pressure, at a temperature of 140 °C for 12 hours. After the screen-printing procedure, the electrode thickness was measured to be 0.008 ± 0.002 mm. This measurement was obtained using a digital thickness gauge at ten different points across the electrode surface to account for potential variability in thickness.

5 MADAP analysis

Our analysis package, MADAP, is further expanded with voltammetry tests, integrating it into our Auto-MISCHBARES framework to facilitate the on-the-fly characterization capabilities (Fig. 4). In our case study, we illustrate the application of the cyclic voltammetry (CV) class from MADAP's voltammetry module for the real-time analysis of the electrochemical data. The class initiates the process by identifying forward and backward scans and automatically labeling cycle numbers, irrespective of their starting points, to enable accurate visualization of the electrochemical process (see `_find_fwd_bwd_scans` and `_identify_cycles`). The module further utilizes the `find_peaks` method from the `scipy.signal` library to locate the peaks in both cathodic and anodic directions and store this information for subsequent analysis (see `_find_peak_currents`). This includes calculating peak-to-peak separation as the absolute distance between the cathodic and anodic peak voltages. Additionally, the half-wave potential is determined by averaging the voltages of corresponding peaks, subsequently used for finding a linear fit with `numpy.polyfit`, from which the half-wave current is derived (see `_calculate_E_half`). The module extends its analysis to compute overpotential, as all the requisite parameters are now available (see `_find_overpotential`). For reactions considered reversible, it calculates the diffusion coefficients, defaulting to a standard temperature of 298 K unless otherwise specified, utilizing the Randles-Sevcik equation to elucidate electrochemical reaction kinetics¹⁷ (see `_calculate_diffusion_coefficient`). This class also quantifies peak currents by identifying the linear representation of the capacitive region through a windowed linear fit, with the fit's quality evaluated by the coefficient of determination (r-squared) value. This approach determines the height of the peak currents relative to this baseline for both cathodic and anodic sweeps (see `_find_height_of_cathodic_peak_current` and `_find_height_of_anodic_peak_current`). Although not the primary focus of our study, the module provides insights into Tafel plot parameters and corrosion point (see `_find_tafel_region` and `_calculate_corrosion_point`). It can generate up to five types of plots, including E-t, I-t, peak parameters versus scan rates, I-V, and Tafel plot, demonstrating its robustness in visual data representation (see `plot`). Finally, the class supports the generation of detailed reports, encapsulating both raw data and analyzed results in CSV and JSON formatted files, respectively (see `save_data`). Additional documentation about this package and the code details can be found in <https://pypi.org/project/MADAP/> and <https://fuzhanrahmanian.github.io/MADAP/> and in GitHub¹⁸.

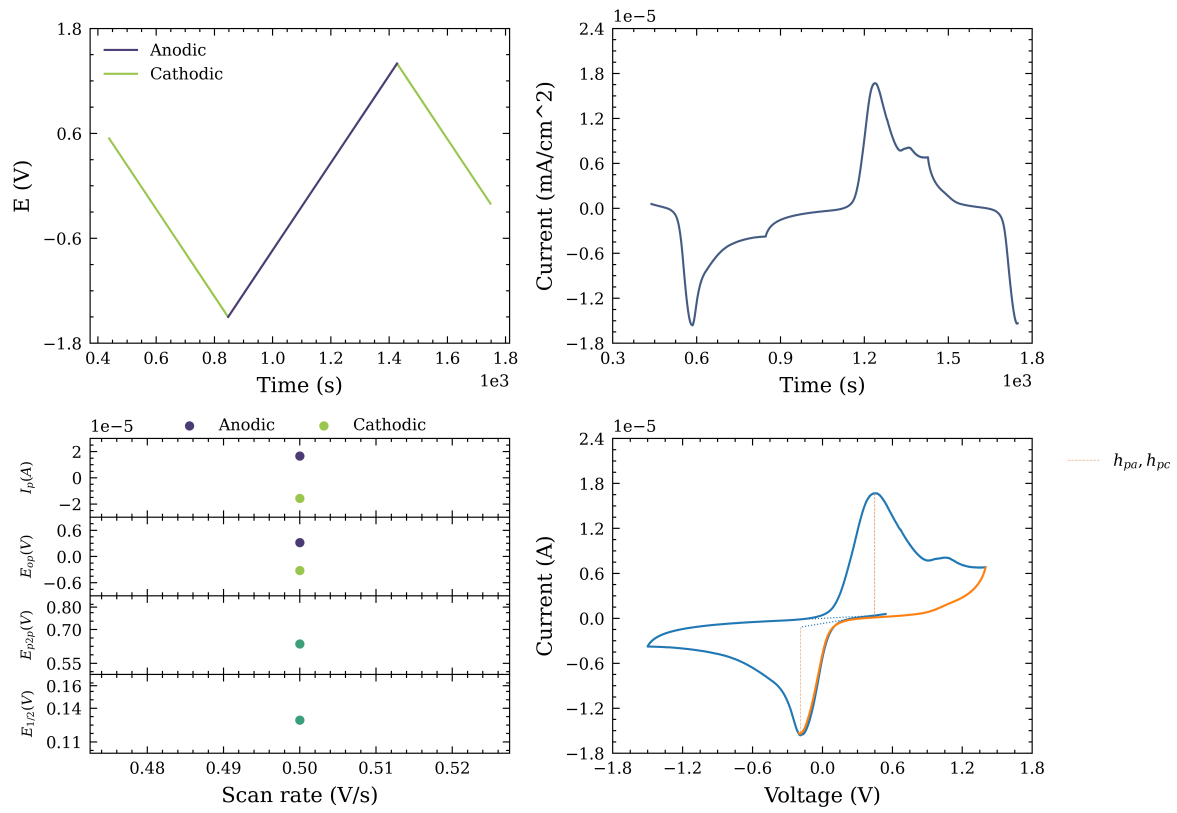


Figure 4: Visualization showcase of sample 6 from set 1, measured with Auto-MISCHBARES and analyzed through MADAP during CV test. This analysis delineates parameters such as anodic and cathodic peaks and half-wave information alongside capacitive and Faradaic current components derived from this package¹⁸.

6 XPS

X-ray photoelectron spectra were recorded under high vacuum conditions using a near-ambient pressure x-ray photoelectron spectroscopy (NAP-XPS) system EnviroESCA from Specs equipped with an Al- K_{α} source (1486.71 eV) operated at 15 kV, 43 W (3 mA emission) and a Phoibos 150 NAP hemispherical analyzer. The base pressure was 1×10^{-7} mbar in the analysis chamber and 1×10^{-9} mbar in the analyzer section. This NAP-XPS is part of the Platform for accelerated electrochemical energy storage Research (PLACES/R) at Helmholtz Institute Ulm¹⁹. To avoid contact with air, the sample environment of the NAP-XPS is directly connected to the glovebox in which the electrochemical measurements were performed. High-resolution spectra were recorded using a pass energy of 30 eV. Peak fitting was performed with CasaXPS version 2.3.24PR1.0 using a Shirley type background and 70% Gaussian and 30% Lorentzian profiles²⁰.

6.1 Spectra

In the following, the XPS spectra for the remaining samples 2 to 6 of the first experimental set are listed.

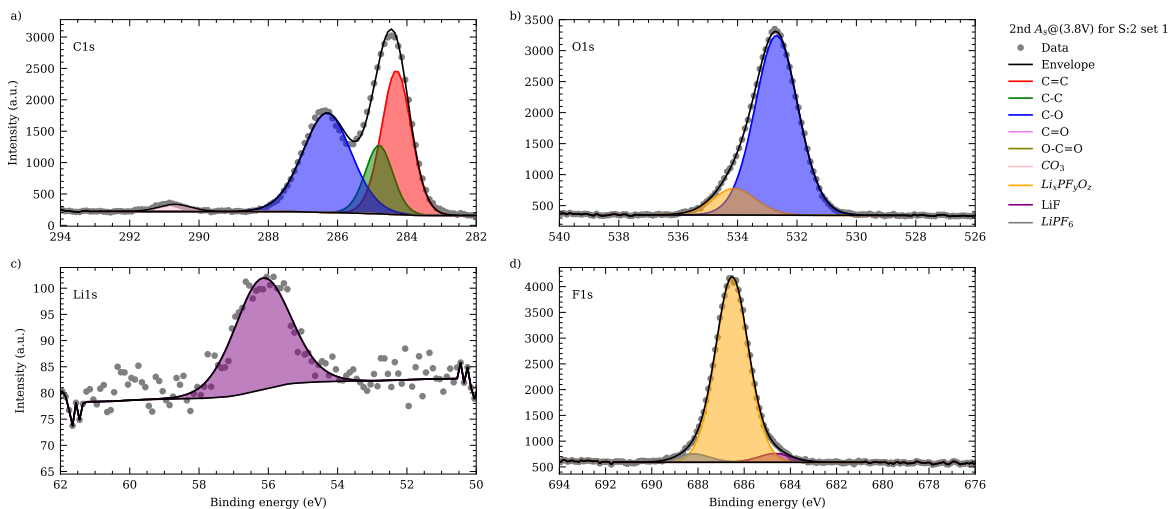


Figure 5: Schematic of X-ray photoelectron spectroscopy (XPS) spectra of the synthesized cathode electrolyte interphase (CEI) on sample 2 from the first set of experiments, captured during the second anodic scan in CV test with a stopping potential value of 3.8 V. This figure illustrates the diverse chemical composition of this layer with peaks corresponding to various functional groups and species: a) The C1s region demonstrates multiple peaks indicative of carbon-based species, b) the O1s region. c) The Li1s region shows the presence of lithium-containing compounds, d) the F1s region is characterized by peaks associated with fluorinated species. Each chemical state identified is denoted by a distinct color in the spectra. The overlaid black line represents the envelope of the aggregated measured data, indicating the sum of contributions from all fitted peaks.

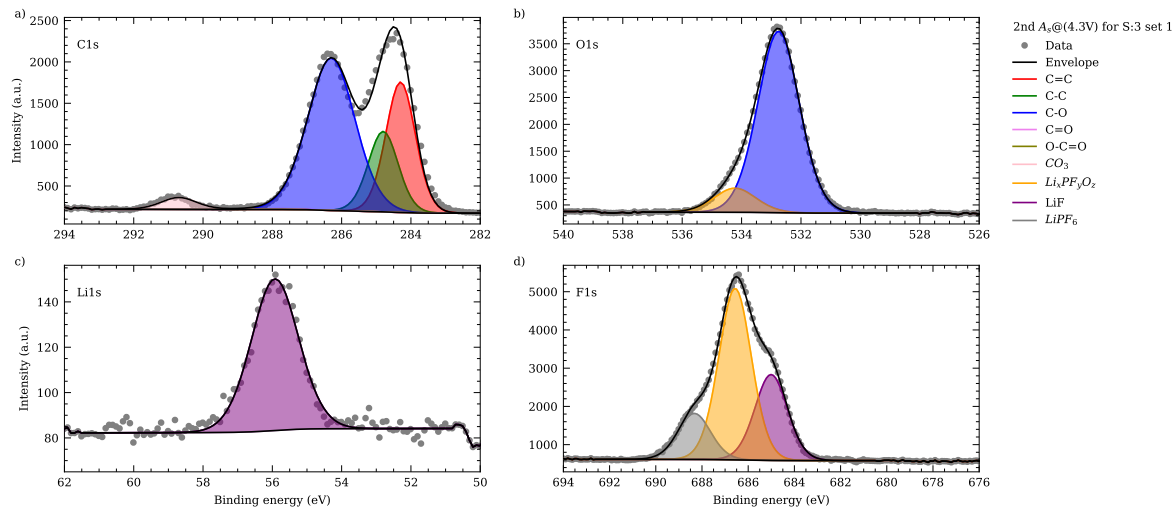


Figure 6: Schematic of XPS spectra of the synthesized CEI on sample 3 from the first set of experiments, captured during the second anodic scan in CV test with a stopping potential value of 4.3 V, This figure illustrates the diverse chemical composition of this layer with peaks corresponding to various functional groups and species: a) The C1s region demonstrates multiple peaks indicative of carbon-based species, b) the O1s region. c) The Li1s region shows the presence of lithium-containing compounds, d) the F1s region is characterized by peaks associated with fluorinated species. Each chemical state identified is denoted by a distinct color in the spectra. The overlaid black line represents the envelope of the aggregated measured data, indicating the sum of contributions from all fitted peaks.

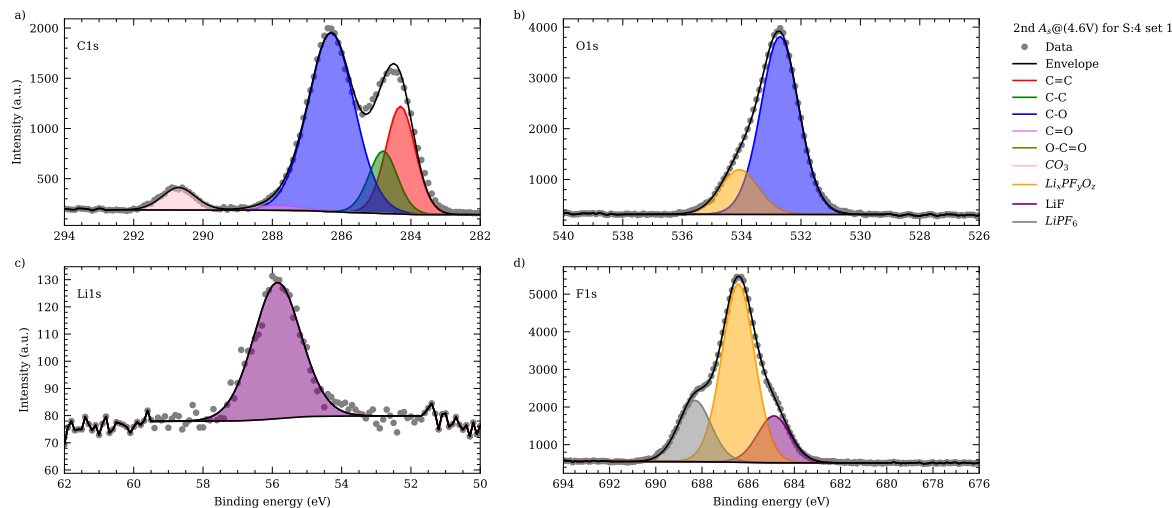


Figure 7: Schematic of XPS spectra of the synthesized CEI on sample 4 from the first set of experiments, captured during the second anodic scan in CV test with a stopping potential value of 4.6 V, This figure illustrates the diverse chemical composition of this layer with peaks corresponding to various functional groups and species: a) The C1s region demonstrates multiple peaks indicative of carbon-based species, b) the O1s region. c) The Li1s region shows the presence of lithium-containing compounds, d) the F1s region is characterized by peaks associated with fluorinated species. Each chemical state identified is denoted by a distinct color in the spectra. The overlaid black line represents the envelope of the aggregated measured data, indicating the sum of contributions from all fitted peaks.

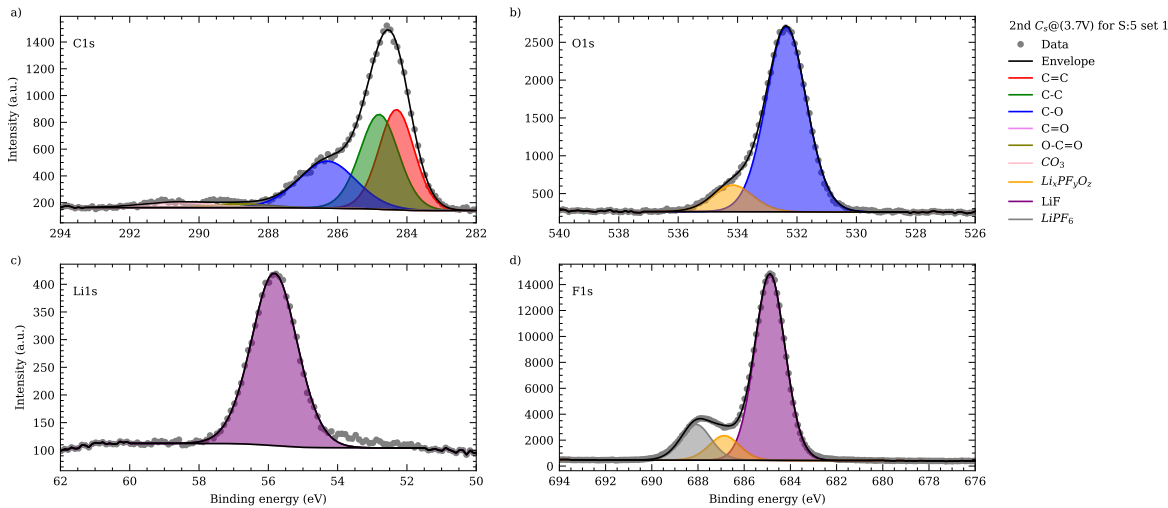


Figure 8: Schematic of XPS spectra of the synthesized CEI on sample 5 from the first set of experiments, captured during the second anodic scan in CV test with a stopping potential value of 3.7 V, This figure illustrates the diverse chemical composition of this layer with peaks corresponding to various functional groups and species: a) The C1s region demonstrates multiple peaks indicative of carbon-based species, b) the O1s region. c) The Li1s region shows the presence of lithium-containing compounds, d) the F1s region is characterized by peaks associated with fluorinated species. Each chemical state identified is denoted by a distinct color in the spectra. The overlaid black line represents the envelope of the aggregated measured data, indicating the sum of contributions from all fitted peaks..

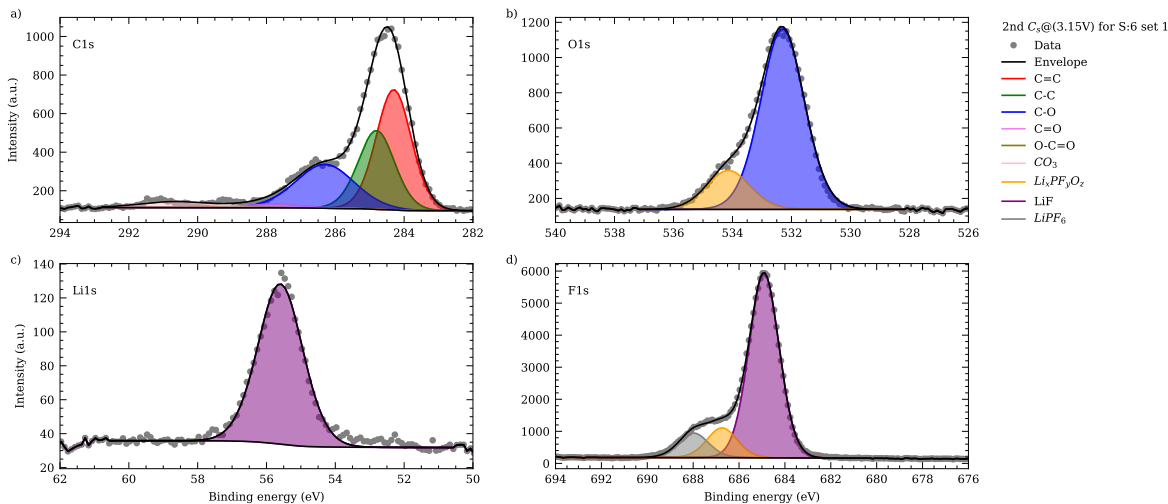


Figure 9: Schematic of XPS spectra of the synthesized CEI on sample 6 from the first set of experiments, captured during the second anodic scan in CV test with a stopping potential value of 3.15 V, This figure illustrates the diverse chemical composition of this layer with peaks corresponding to various functional groups and species: a) The C1s region demonstrates multiple peaks indicative of carbon-based species, b) the O1s region. c) The Li1s region shows the presence of lithium-containing compounds, d) the F1s region is characterized by peaks associated with fluorinated species. Each chemical state identified is denoted by a distinct color in the spectra. The overlaid black line represents the envelope of the aggregated measured data, indicating the sum of contributions from all fitted peaks.

Table 1: To evaluate the fit quality of XPS data, two metrics, namely Residual Standard Deviation (RSD) and Goodness of Fit, are provided for every spectral region across all samples.

Sample	Region	Goodness of Fit	Residual STD
S:1, set 1	C1s	239.208	0.854
	O1s	320.822	1.079
	F1s	1505.901	2.661
	Li1s	416.715	1.534
S:2, set 1	C1s	990.612	2.094
	O1s	329.004	0.810
	F1s	448.093	0.883
	Li1s	214.526	0.794
S:3, set 1	C1s	1128.550	2.351
	O1s	419.031	1.134
	F1s	847.567	1.325
	Li1s	243.398	0.854
S:4, set 1	C1s	761.609	1.998
	O1s	441.226	1.243
	F1s	614.448	1.081
	Li1s	195.243	0.823
S:5, set 1	C1s	303.729	1.064
	O1s	413.421	1.241
	F1s	1926.761	3.194
	Li1s	543.616	1.778
S:6, set 1	C1s	271.224	1.089
	O1s	313.175	1.175
	F1s	735.157	2.029
	Li1s	227.720	1.163

References

- [1] F. Rahmanian, J. Flowers, D. Guevarra, M. Richter, M. Fichtner, P. Donnelly, J. M. Gregoire and H. S. Stein, *Advanced Materials Interfaces*, 2022, **9**, 2101987.
- [2] S. Ramírez, *FastAPI*, <https://github.com/tiangolo/fastapi>.
- [3] T. Christie, *Uvicorn*, <https://github.com/encode/uvicorn>.
- [4] M. Grinberg, *Flask web development: developing web applications with python*, " O'Reilly Media, Inc.", 2018.
- [5] Bokeh Development Team, *Bokeh: Python library for interactive visualization*, 2018.
- [6] *WebSockets*, <https://github.com/python-websockets/websockets/tree/main>.
- [7] *pythonnet - Python.NET*, <https://github.com/pythonnet/pythonnet>.
- [8] C. R. Harris, K. J. Millman, S. J. van der Walt, R. Gommers, P. Virtanen, D. Cournapeau, E. Wieser, J. Taylor, S. Berg, N. J. Smith, R. Kern, M. Picus, S. Hoyer, M. H. van Kerkwijk, M. Brett, A. Haldane, J. F. del Río, M. Wiebe, P. Peterson, P. Gérard-Marchant, K. Sheppard, T. Reddy, W. Weckesser, H. Abbasi, C. Gohlke and T. E. Oliphant, *Nature*, 2020, **585**, 357–362.
- [9] W. McKinney *et al.*, Proceedings of the 9th Python in Science Conference, 2010, pp. 51–56.
- [10] *pgAdmin*, <https://www.pgadmin.org/>.
- [11] F. Di Gregorio, *psycopg2 - Python-PostgreSQL Database Adapter*, <https://github.com/psycopg/psycopg2>.
- [12] G. Bradski, *Dr. Dobbs's Journal of Software Tools*, 2000, –.
- [13] F. Rahmanian, *MADAP*, <https://github.com/fuzhanrahmanian/MADAP>.
- [14] F. Pedregosa, G. Varoquaux, A. Gramfort, V. Michel, B. Thirion, O. Grisel, M. Blondel, P. Prettenhofer, R. Weiss, V. Dubourg, J. Vanderplas, A. Passos, D. Cournapeau, M. Brucher, M. Perrot and E. Duchesnay, *Journal of Machine Learning Research*, 2011, **12**, 2825–2830.
- [15] P. Virtanen, R. Gommers, T. E. Oliphant, M. Haberland, T. Reddy, D. Cournapeau, E. Burovski, P. Peterson, W. Weckesser, J. Bright, S. J. van der Walt, M. Brett, J. Wilson, K. J. Millman, N. Mayorov, A. R. J. Nelson, E. Jones, R. Kern, E. Larson, C. J. Carey, Í. Polat, Y. Feng, E. W. Moore, J. VanderPlas, D. Laxalde, J. Perktold, R. Cimrman, I. Henriksen, E. A. Quintero, C. R. Harris, A. M. Archibald, A. H. Ribeiro, F. Pedregosa, P. van Mulbregt and SciPy 1.0 Contributors, *Nature Methods*, 2020, **17**, 261–272.
- [16] H. Krekel, B. Oliveira, R. Pfannschmidt, F. Bruynooghe, B. Laughner and F. Bruhin, *pytest x.y*, 2004, <https://github.com/pytest-dev/pytest>.
- [17] A. J. Bard, L. R. Faulkner and H. S. White, *Electrochemical methods: fundamentals and applications*, John Wiley & Sons, 2022.
- [18] F. Rahmanian, *Modular and Autonomous Data Analysis Platform (MADAP)*", 2023, <https://doi.org/10.5281/zenodo.10357192>.
- [19] H. S. Stein, A. Sanin, F. Rahmanian, B. Zhang, M. Vogler, J. K. Flowers, L. Fischer, S. Fuchs, N. Choudhary and L. Schroeder, *Current Opinion in Electrochemistry*, 2022, **35**, 101053.
- [20] N. Fairley, V. Fernandez, M. Richard-Plouet, C. Guillot-Deudon, J. Walton, E. Smith, D. Flahaut, M. Greiner, M. Biesinger, S. Tougaard *et al.*, *Applied Surface Science Advances*, 2021, **5**, 100112.